Heating Measurements on Space Shuttle Orbiter Models with Differentially Deflected Elevons

William L. Wells*
NASA Langley Research Center, Hampton, Virginia

The phase-change paint technique was used to make heat-transfer measurements on five Space Shuttle Orbiter models with differentially deflected elevons. The outboard elevons were deflected windward through an angle δ when the inboard elevons were deflected through an angle -2δ, where $\delta = 0$, 5, 10, 15, and 20 deg. The models were tested in air at Mach 6 and 10 with two different flow conditions at each Mach number. Each test was run at three angles of attack: 20, 28, and 35 deg. This study was restricted to the windward side of the wing/elevon area. Multiple chordwise streaks of high heating often occurred on the wings and sometimes extended to localized spots of high heating on the windward-deflected elevons. The extent of heating was a function of angle of attack and test conditions, but, in general, differential deflection of the elevons affected the wing heat-transfer coefficient on the order of 40% or less, whereas the windward elevon heat-transfer coefficient was a function of the deflection angle and could be many times the value determined for the undeflected elevon.

Nomenclature

c = specific heat of model material, W-s/K
h = convective heat-transfer coefficient, W/m^2K
k = thermal conductivity of model material, W/m-K
L = total length of model excluding body flap, m
l = length of chord (includes elevon), m
M = Mach number, dimensionless
$N_{Re,L}$ = freestream Reynolds number
P = pressure, Pa
Pr = Prandtl number, dimensionless
$\dot{q}$ = convective heating rate, W/m^2
r_c = recovery factor, dimensionless
T = temperature, K
$\bar{T}$ = temperature ratio defined by Eq. (2)
t = time, s
X = centerline distance from model nose to a particular location, m
x = distance from wing leading edge along chord, m
α = thermal diffusivity of model material, m^2/s
α = model angle of attack, deg
β = defined by Eq. (3)
γ = ratio of specific heats for air
δ = angle between wing chord line and the outboard elevon chord line, deg
ρ = density of model material, kg/m^3

Subscripts

aw = adiabatic wall
i = initial
L = total length of model excluding body flap
max = maximum
pc = phase change
t = total
0 = reference
δ = elevon deflection-angle dependent

Presented as Paper 83-1534 at the AIAA 18th Thermophysics Conference, Montreal, Canada, June 1-3, 1983; received July 5, 1983; revision received Feb. 15, 1984. This paper is declared a work of the U.S. Government and therefore is in the public domain.

*Aero-Space Technologist, Aerothermodynamics Branch, Space Systems Division.

Introduction

THE Space Shuttle Orbiter flies most of its entry trajectory at a high angle of attack (about 40 deg) such that the rudder is ineffective for yaw control. Yaw jets mounted near the aft end of the Orbiter are presently used to provide this control, although the fuel required to provide this function results in additional weight that otherwise could be used for payload. An unpublished theoretical study at Langley Research Center has indicated that over at least part of the entry trajectory yaw control could be achieved by differential deflection of the elevons. Differential deflection is defined herein as a downward (into the wind) deflection of the outboard elevons and an upward deflection of the inboard elevons. An effective configuration considered in the theoretical study utilized downward deflected outboard elevons at an angle δ and inboard elevons deflected at an angle -2δ, but with δ different on opposite sides of the vehicle. This configuration was predicted to provide yaw control equal to the yaw jets at $M = 10$, better control at lesser Mach numbers, and significant control at Mach numbers somewhat greater than 10. During the portion of the entry trajectory when aerodynamic heating is significant, present flight procedures call for inboard and outboard elevon deflections to be in the same direction and through relatively small angles (up to about 6 deg on flights 1-4).[1]

This paper reports on a series of wind tunnel heat-transfer tests conducted to ascertain the effect on aerodynamic heating of the Orbiter elevons due to differential deflection. Heating on the wings forward of the elevons was also measured. The phase-change paint heat-transfer technique was used, and the study was restricted to the windward surface.

Experimental Method

Models

A glassy-ceramic material was used to cast five 1%-scale Orbiter models. Each model had elevons that were deflected at angles different from the other four models. The five outboard deflection angles were: 0, 5, 10, 15, and 20 deg downward. The corresponding inboard deflection angles were: 0, 10, 20, 30, and 40 deg upward. To provide redundancy in heat-transfer measurements, the port and starboard deflection angles were the same on each model since flow symmetry was expected. The correct geometry was maintained on the windward side of

Table 1 Nominal values of wind tunnel parameters

Mach. No.	$N_{Re,L}$, $\times 10^6$	T_t, K	T_{static} K	P_t, kPa	P_{static}, kPa
6	2.15	500	62	827.4	0.55
6	4.27	506	62	1723.7	1.09
10	0.54	1011	52	2413.2	0.076
10	2.15	1011	50	10066.3	0.214

the elevons, but they were made thicker on the leeward side so that the one-dimensional heat-transfer approximation could be used in the heating analysis. Each model was made with an undeflected body flap, and a hollow stainless-steel sting was installed coaxial with the fuselage centerline at the time the model was cast. The sting also served as a conduit for leads of a thermocouple that was cast into the material at the fuselage centerline just aft of the Orbiter canopy.

Scope of Tests

The tests were conducted in air in two wind tunnels: the 20-in. Mach 6 Tunnel and the Continuous Flow Hypersonic ($M = 10$) Tunnel, both at the Langley Research Center. Each model was tested in two flow environments characterized by the Reynolds number. Pertinent test conditions for all flow environments of interest are listed in Table 1. Each model was tested at angles of attack of 20, 28, and 35 deg in each flow environment. The models were injected into the test stream at the desired angle of attack after tunnel flow conditions were established.

Facilities

The Langley 20-in. Mach 6 Tunnel is a blowdown wind tunnel that uses dry air as the test gas. The air is heated to the desired total temperature by electrical resistance heaters. A fixed-geometry, two-dimensional, contoured nozzle is used. The side walls are parallel, forming a 52×52 cm test section. A description of this facility and calibration data can be found in Refs. 2-4.

The Langley Continuous Flow Hypersonic Tunnel, described in Ref. 5, was used in a blowdown mode for the test series reported here. This tunnel also uses dry air which is heated to the total temperature by electrical resistance heaters. The three-dimensional, rectangular nozzle expands to a test section that is 79 cm square by 86 cm long.

Heat-Transfer Measurement Technique

The phase-change paint technique employs a series of paints that melt or change phase at known temperatures. Typically, a thin coat of light-colored paint is sprayed on a dark-colored model. The unmelted paint is opaque but becomes transparent when melted. Knowledge of the model material properties, the time required to melt the paint, and the paint melt temperature provides sufficient information to determine the heat-transfer coefficient at a particular location. Reference 6 presents a comprehensive discussion of this technique. Only those portions that are directly applicable to this study are briefly discussed here.

Mathematical relations sufficient to determine the heat-transfer coefficient can be derived from the equations governing transient one-dimensional heat conduction into a semi-infinite slab. These derived relations are

$$\bar{T} = 1 - e^{\beta^2}\operatorname{erfc}\beta \tag{1}$$

where

$$\bar{T} = \frac{T_{pc} - T_i}{T_{aw} - T_i} \tag{2}$$

and

$$\beta = h/k \propto t \quad \text{or} \quad h = \beta\sqrt{\rho ck/t} \tag{3}$$

The model material properties parameter $\sqrt{\rho ck}$ was determined experimentally by use of the heating device described in Ref. 7. In that device, a sample of model material and a calorimeter were exposed simultaneously to a step heat input and the material properties were related to the measured temperature response. The parameter β was found from Eqs. (1) and (2), and the time t required to melt the paint at a particular location was determined from the known framing rate of motion-picture film exposed during a test. The adiabatic wall temperature in Eq. (2) was obtained from

$$T_{aw} = \frac{T_{aw}}{T_t}T_t = \frac{1 + r_c(\gamma - 1/2)M^2}{1 + (\gamma - 1/2)M^2}T_t$$

$$= \frac{1 + \sqrt{Pr}(\gamma - 1/2)M^2}{1 + (\gamma - 1/2)M^2}T_t \tag{4}$$

which assumes a constant-property, laminar boundary-layer flow condition. The flow over the wings and elevons was found to be very complex and determination of a correct local M seemed unlikely with the present data; therefore, the freestream Mach number was used to calculate T_{aw}. Using M that is about one-third the freestream value, in either tunnel, would result in an increase in T_{aw} of about 6.5%. The total temperature T_t was obtained from wind tunnel thermocouples, and the model initial temperature T_i was measured by the thermocouple that was embedded in the model when it was cast. Enough time was allowed between tests for T_i to return to the ambient temperature.

For a particular test, a paint was selected with a phase-change temperature that would allow the data to be obtained before the thermal diffusion time was exceeded in the thinnest wall section of the model. This requirement derives from a boundary condition imposed on the original semi-infinite slab approximation. The diffusion time in the thinnest section, which was at the elevon hinge line, was about 12 s. Most test times were on the order of 10 s. Thicker sections could have accommodated longer test times. On the other hand, care was taken not to compromise data accuracy by selecting a melt temperature so low that $(T_{pc} - T_i)$ in Eq. (2) would be very small or that the model injection time, when conditions are transient, would be a large portion of the data-gathering time at any particular location on the model. In some instances, it was necessary to use a paint on the elevons with melt temperature different from the rest of the model.

The motion-picture camera used to record the data was operated at a rate of 10 frame/s. A stroboscopic lamp was used to illuminate the model, and the pulse rate was synchronized with the camera framing rate. Continuous-operating high-intensity lamps can add a significant radiant heat load to the model.[6]

Data Reduction and Accuracy

From images recorded on motion-picture film, the boundary between melted and unmelted paint at a particular time during a test was superimposed on an outline of the Orbiter model. This boundary represents a contour line of constant heating rate that is determined by the heat-transfer measurement technique of Ref. 6. At a later test time, the new melt boundary, representing a lesser heating rate, was also superimposed onto the Orbiter outline, and so on, until a heating-rate contour map of the windward wing and elevon surfaces was obtained. The area between two contour lines has heating rates that have upper and lower limits defined by the two lines. The data presented here are in terms of the heat-transfer coefficient that has been nondimensionalized by the theoretical stagnation-point coefficient[8] for a 0.305-m (1-ft) radius sphere at the model scale and test conditions. The reference h_0 was based on a wall temperature of 294.4 K.

Factors that affect the data accuracy are discussed at length in Ref. 6. These factors are too numerous and variable to

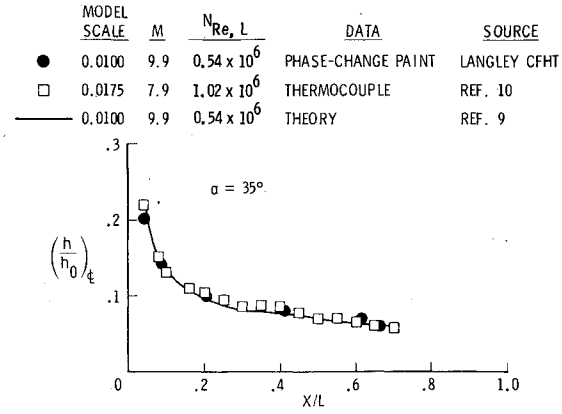

Fig. 1 Comparison of data obtained from theory and the experimental techniques of phase-change paint and thermocouples on thin metal skin along the Orbiter centerline.

elaborate on in this paper but include model injection time, time at which data is read, $(T_{pc} - T_i)$, known value of T_{pc}, model material properties, and determination of initial time of heating ($t = 0$). Model illumination, camera viewing angle, and the heating gradient over a particular surface area were also found to affect the accuracy with which the data could be read from the film. Rather than try to evaluate each factor and its contribution to errors, the present phase-change data were compared to theory[9] for the same configuration and test conditions, and also to experimentally obtained thermocouple data[10] for very nearly the same conditions. Figure 1 presents a comparison of the different methods for the Orbiter fuselage centerline at $\alpha = 35$ deg. The methods can be seen to agree within about 5% over most of the data span, and only when data read times are short (at highest h/h_0) do theory and phase-change data disagree by about 10%. Thermocouple and phase-change data continue to be in close agreement throughout the data range.

Results and Discussion

The highest heating rate for any case occurred along the leading edge of the wings and along the inboard edge of the outboard elevons. Values of heating rate were not obtained in these localized areas because the paint melted almost immediately upon entry into the test stream. Furthermore, these areas soon developed a thin char layer that resulted in unknown material properties. The inboard elevons that were deflected leeward never received enough heating to melt the paint. The inboard elevons and wings were always painted with the same paint for a particular test. The outboard elevons sometimes received heating that was higher than the wing and therefore required paint with a higher melting temperature so that the wing and elevon paint melt times would both fall within the limit specified by the data analysis technique.

Geometric patterns of heating over the wings and outer elevons were often complex. At Mach 6, the highest heating (excluding the leading edge) sometimes occurred at a spot near the center of the wing. In many other instances, at both Mach 6 and 10, high heating occurred in multiple chordwise streaks on the wings, and these streaks often extended to spots of high heating on the windward deflected elevons. Examples of multiple-streak and spot heating patterns are shown by single frames of motion-picture film in Fig. 2. The dark areas indicate melted paint and areas of high heating (except for shadows as indicated). There were some variations in the heating patterns that were dependent to some degree on the Mach and Reynolds numbers, but for the most part these patterns were similar for a particular angle of attack. The major exception was the spot of high heating near the wing center that was noted in Fig. 2b. This occurred only at Mach 6

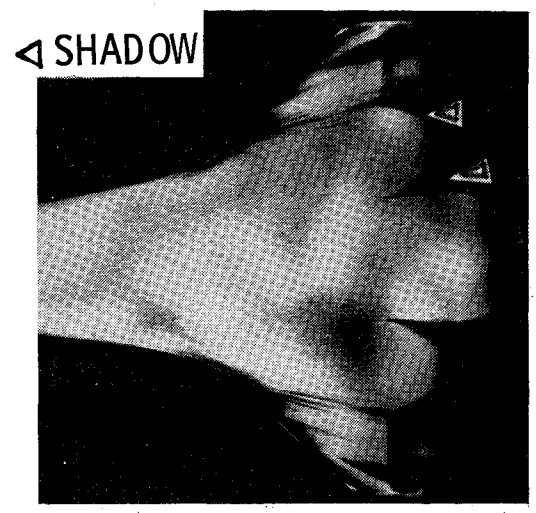

a) $M = 6$, $N_{Re,L} = 2.1 \times 10^6$, $\alpha = 28$ deg, $\delta = 5$ deg.

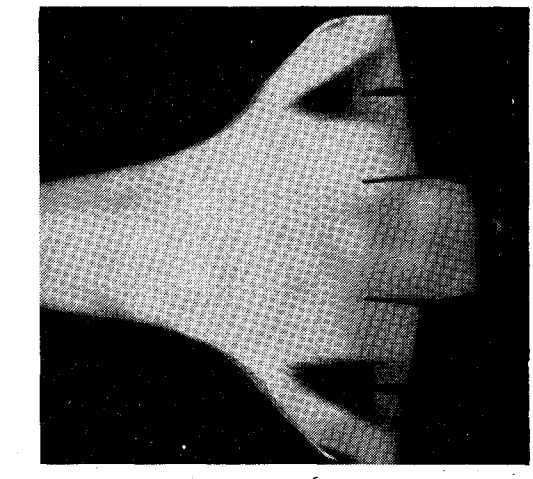

b) $M = 6$, $N_{Re,L} = 4.2 \times 10^6$, $\alpha = 35$ deg, $\delta = 0$ deg.

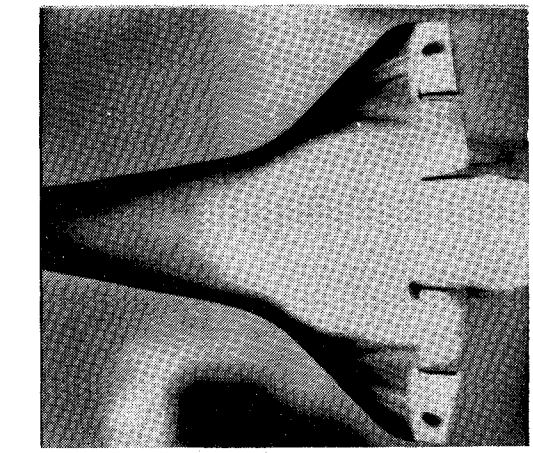

c) $M = 10$, $N_{Re,L} = 2.1 \times 10^6$, $\alpha = 28$ deg, $\delta = 15$ deg.

Fig. 2 Single frames of motion pictures showing examples of paint melt patterns. Dark areas indicate melted paint.

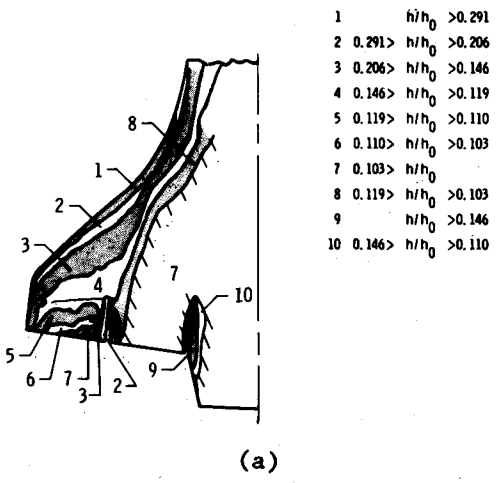

(a)

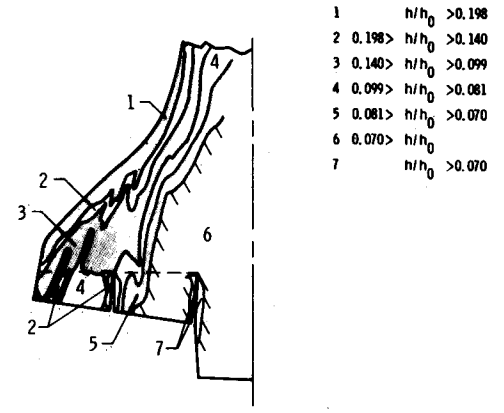

(b)

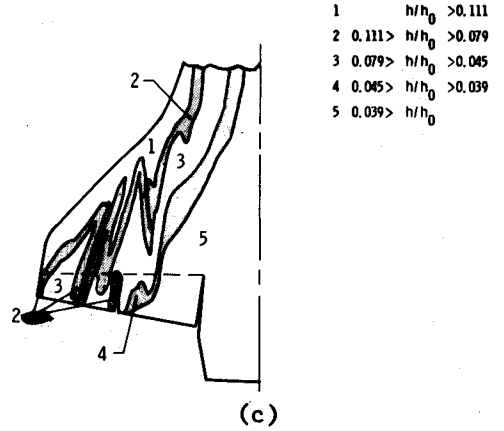

(c)

Fig. 3 Heat-transfer coefficients and heating patterns on the Orbiter wing and elevons at $M = 10$, $N_{Re,L} = 2.1 \times 10^6$, $h_0 = 0.114$ W/cm^{2}K, and $\delta = 0$ deg: a) $\alpha = 35$ deg; b) $\alpha = 28$ deg; c) $\alpha = 20$ deg.

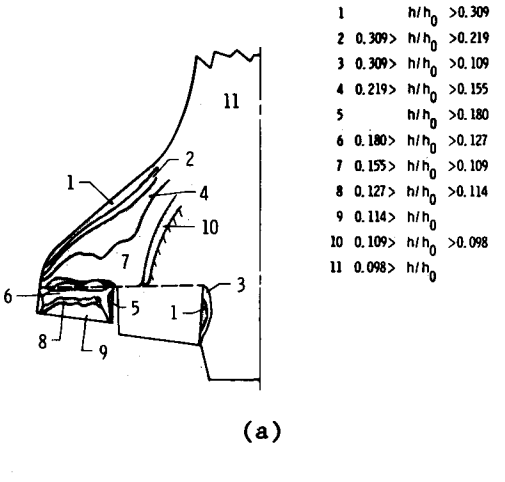

(a)

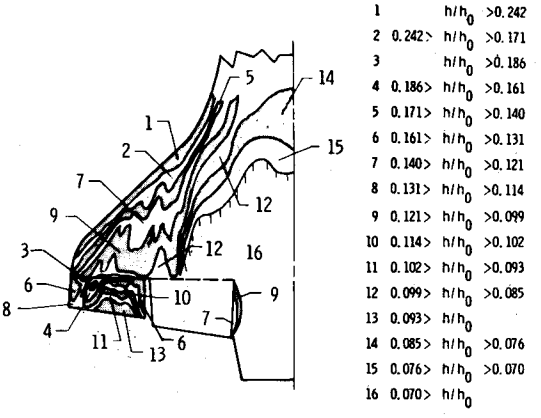

(b)

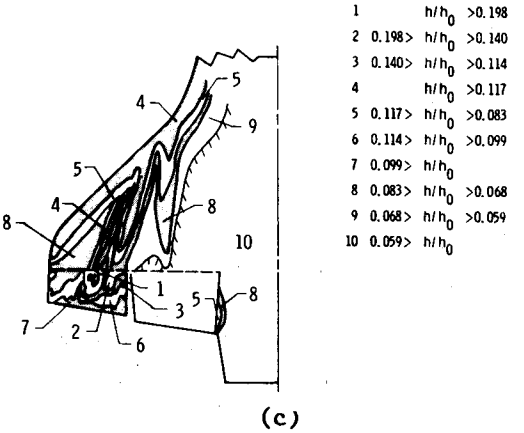

(c)

Fig. 4 Heat-transfer coefficient and heating patterns on the Orbiter wing and elevons at $M = 10$, $N_{Re,L} = 2.1 \times 10^6$, $h_0 = 0.114$ W/cm^{2}K, and $\delta = 10$ deg; a) $\alpha = 35$ deg; b) $\alpha = 28$ deg; c) $\alpha = 20$ deg.

with the highest N_{Re} and with $\delta = 0$, but at all three values of α. Deflection of the elevons resulted in a change in the pattern to ones more nearly like those observed in other cases. Because of space limitations, only selected (h/h_0) contour maps are presented here.

Values of heat-transfer coefficient and geometrical patterns of heating over the wing and outer elevon obtained from some of the Mach 10 tests are shown in Figs. 3-5. The data are shown for only one side of the model since the heating was symmetrical about the model centerline. The data are presented as ranges of nondimensionalized heat-transfer coefficients that are within a certain outlined area on the wing or elevon. The data are shown for a nominal $N_{Re,L} = 2.10 \times 10^6$.

When $\alpha = 35$ deg (Figs. 3a, 4a, and 5a), the heat-transfer coefficient patterns are simple and heating decreases in a direction approximately normal to the wing leading edge. When $\alpha = 28$ and 20 deg (b and c of Figs. 3-5), however, chordwise streaks of high heating develop on the wing and extend to the outboard elevon. There is little apparent effect on wing heating patterns when the elevons are deflected

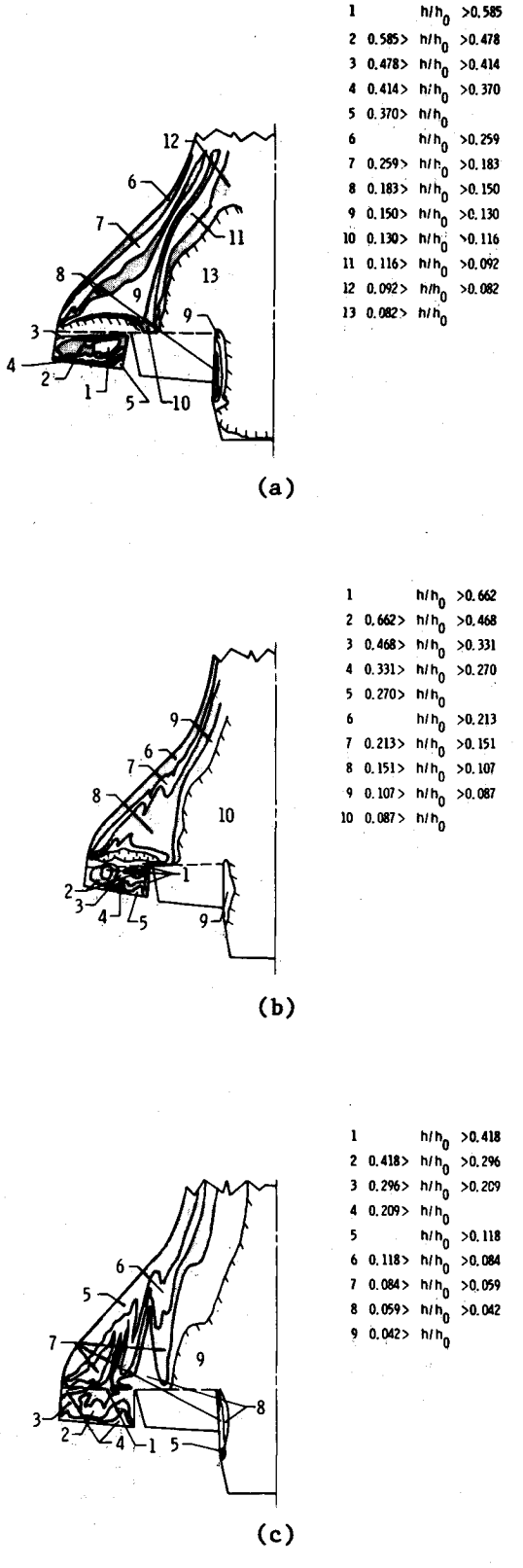

Fig. 5 Heat-transfer coefficients and heating patterns on the Orbiter wing and elevons at $M = 10$, $N_{Re,L} = 2.1 \times 10^6$, $h_0 = 0.114$ W/cm^{2}K, and $\delta = 20$ deg; a) $\alpha = 35$ deg; b) $\alpha = 28$ deg; c) $\alpha = 20$ deg.

through any angle δ, but apparently some feature in the flow structure intersects the windward deflected elevon which results in localized spots of high heating on that surface, particularly at $\alpha = 20$ and 28 deg. The nature of the flow structure responsible for the streaks or spots of high heating is not known at this time, but it is thought to originate with interaction of shocks from the bow, strake, and wing.

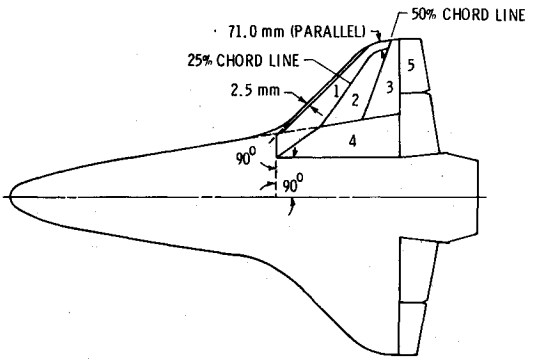

Fig. 6 Location of panels on the Orbiter models.

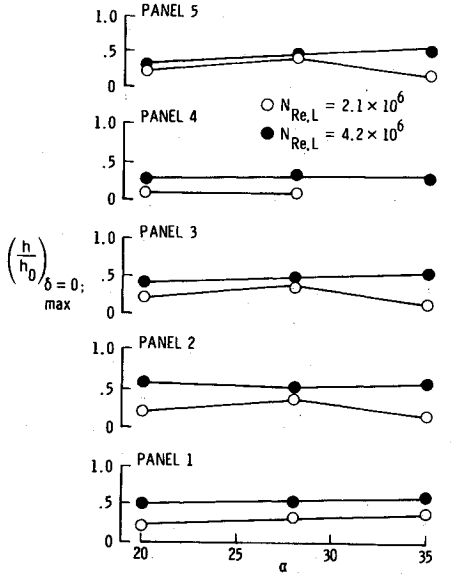

Fig. 7 Maximum heat-transfer coefficient that occurs anywhere on each panel when $\delta = 0$ and $M = 6$ at all three α.

The information in Figs. 3-5 represents the basic data. Data in this form provide details of the geometric distribution of heating and may give clues as to the nature of the flow giving rise to the heating rates on various areas. However, it is difficult to identify trends in magnitude of heating rate on the wing and elevon resulting from differential deflections of the elevons. These trends can best be displayed by graphical representation of the data. For the purpose of data presentation, the wing surface is considered to be made up of four panels and the outboard elevon with one panel. The location of these panels is shown in Fig. 6.

The effect of angle of attack and elevon deflection on maximum heating on a particular panel at $M = 6$ is shown in Figs. 7-9. The maximum (h/h_0) was selected from any area of a particular panel provided that value covered as much as approximately 5% or more of the total panel area. The data were taken from the original (h/h_0) contour maps similar to Figs. 3-5. The original figures are larger and somewhat more detailed than Figs. 3-5, however. Figure 7 shows the maximum (h/h_0) on each panel as a function of α when the elevons are not deflected. On most panels at each α, $(h/h_0)_{max}$ for $N_{Re,L} = 4.20 \times 10^6$ is about twice the value for $N_{Re,L} = 2.10 \times 10^6$. The outboard elevon heating, however, is not as sensitive to N_{Re} when $\alpha = 20$ or 28 deg. Apparently this is due to the streaks that extend high heating to the elevons at low α and low N_{Re} but do not at the higher N_{Re}. Actually, at the higher N_{Re}, the heating patterns did not exhibit streaks but appeared more nearly like Fig. 2b. Except for panel 1, the

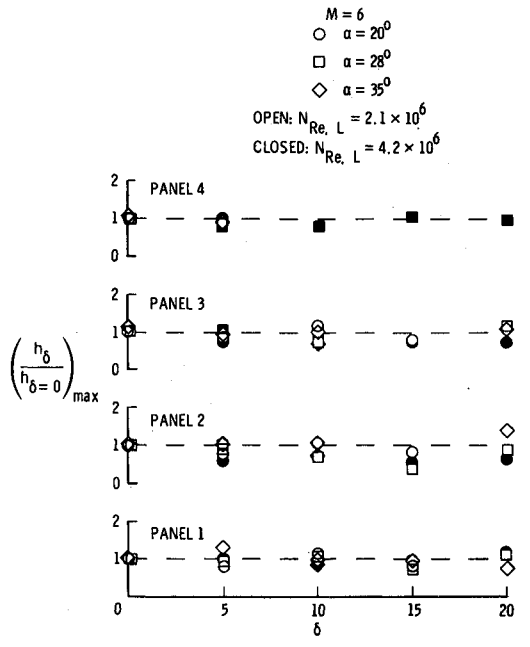

Fig. 8 Effect of elevon deflection δ on the maximum heat-transfer coefficient found anywhere on each of the wing panels when $M = 6$.

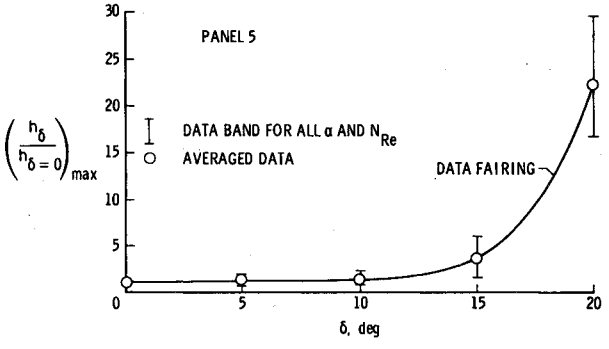

Fig. 9 Effect of elevon deflection δ on the maximum heat-transfer coefficient found anywhere on panel 5 (outboard elevon) when $M = 6$.

lower N_{Re} heating is greatest when $\alpha = 28$ deg, but in most cases, heating continually increases with α at the higher $N_{Re,L}$. The effect of elevon deflection on the heating of the wing panels is shown in Fig. 8. In this plot the maximum heat-transfer coefficient on a panel, that occurred when the outboard elevon was deflected at some angle δ, is compared to the maximum heat-transfer coefficient on that panel when the elevon was undeflected, but at the same α and test conditions. Heating on the most inboard panel (panel 4) was usually the lowest, and in many tests, paint on that panel did not melt within the allotted test time. Furthermore, panel 4 did not exhibit the spots or streaks of high heating often seen on the other wing panels. Consequently, the panel 4 data are limited but probably are representative of the random scatter (about ±15%) in all the data of Fig. 8. Except for one case, panel 2, none of the data for any wing panel obtained when the elevons were deflected differ from $h_{\delta=0}$ data by more than ±40%.

The effect of elevon deflection on heating of the outboard elevon itself is much more profound than on any of the wing panels. The comparison of maximum h for the deflected and undeflected elevon is shown in Fig. 9. These data have been averaged over all α and $N_{Re,L}$ since no obvious correlation between the parameters was discernible. The spread of the data is indicated by brackets. On average, h_δ is no more than

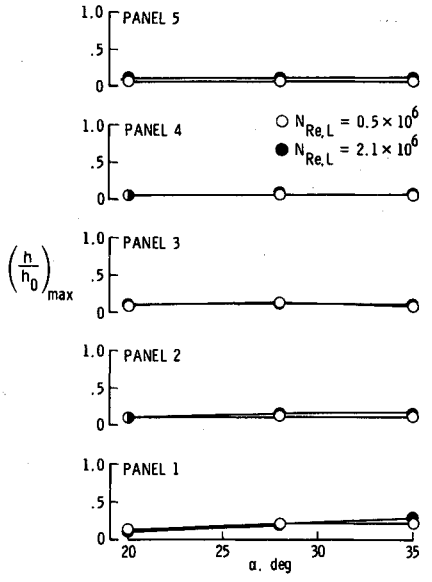

Fig. 10 Maximum heat-transfer coefficient that occurs anywhere on each panel when $\delta = 0$ and $M = 10$.

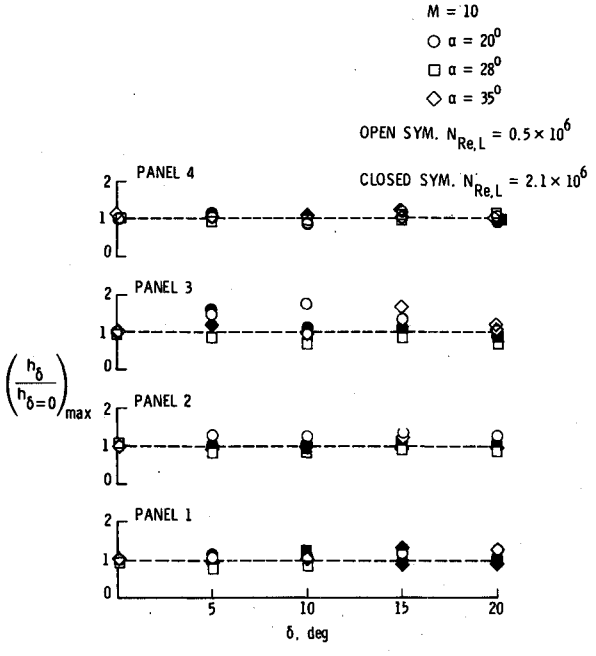

Fig. 11 Effect of elevon deflection δ on the maximum heat-transfer coefficient found anywhere on each of the wing panels when $M = 10$.

50% greater than $h_{\delta=0}$ up to $\delta = 10$ deg. Beyond that deflection, however, h_δ increases rapidly until it is as much as 22 times $h_{\delta=0}$ when $\delta = 20$ deg. Large deflection angles may cause flow separation on the wing and reattachment on the elevon, and in some instances the flow phenomena responsible for the observed streak heating appear to impinge on the highly deflected elevon resulting in increased heating.

Data from the Mach 10 tests are shown in Figs. 10-13. The maximum values of (h/h_0) found anywhere on a particular panel are shown as a function of angle of attack in Fig. 10 for all five panels. These data are for nominal Reynolds numbers of 0.52 and 2.10×10^6, and are from the undeflected elevons tests. Reynolds number effects are small on the wing panels, but on the outboard elevon $(h/h_0)_{max}$ is greater for the higher N_{Re} at all α. The effect of elevon deflection on heating of the wing panels is shown in Fig. 11. Study of the original heating

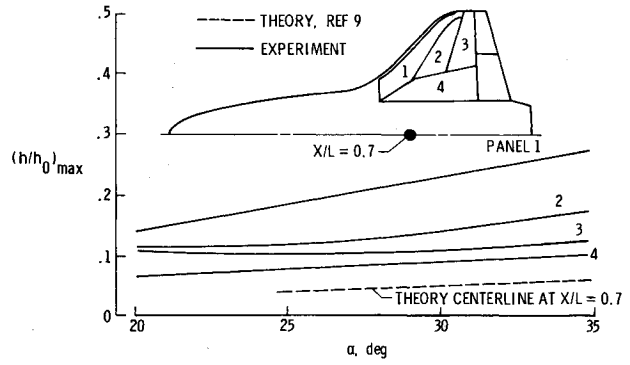

Fig. 12 Comparison of maximum heat-transfer coefficients on all four wing panels and at one point on the Orbiter centerline when $M = 10$.

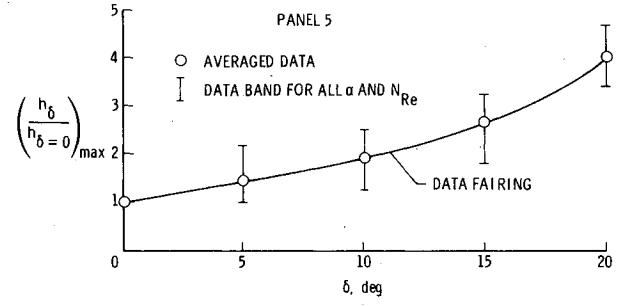

Fig. 13 Effect of elevon deflection δ on the maximum heat-transfer coefficient found anywhere on panel 5 (outboard elevon) when $M = 10$.

contours suggests that increasingly large elevon deflections cause inward turning of the flow (toward the leeward deflected elevon) and even flow separation forward of the windward elevon, thereby changing the heating distribution on the wing to some extent. Heating of panels 1 and 4 is not greatly affected by the change in δ because of their locations. Panels 2 and 3 show more variation of $(h_\delta/h_{\delta=0})_{max}$ with δ although the variation with α (indicated by different symbols) seems more evident. To show the trend in $(h/h_0)_{max}$ as a function of α for all four wing panels, the data for all δ and both N_{Re} were plotted and a curve faired through each set of data. These faired-data curves along with one theoretical curve calculated for a point at $x/L = 0.7$ on the fuselage centerline are shown in Fig. 12. The curves for panels 1 and 4 and the theoretical curve show a linear decrease in $(h/h_0)_{max}$ as α is decreased. Curves for panels 2 and 3 show a similar decrease when α is large (28 deg $< \alpha <$ 35 deg), but $(h/h_0)_{max}$ does not continue to decrease, and even begins to rise somewhat as α decreases from 28 to 20 deg. Although values of $(h/h_0)_{max}$ on panels 2 and 3 do not exceed the values for panel 1, the larger values at lower α may be important in terms of total heat load on the wing for flight missions that require greater cross range and, therefore, smaller α than has previously been flown. Apparently the high heating streaks observed in this study at the lower α extend the high heating levels that normally occur near the wing leading edge farther back on the wing surface.

The effect of δ on $(h/h_0)_{max}$ for the outboard elevon at Mach 10 is shown in Fig. 13. Recall that $(h/h_0)_{max}$ for $\delta = 0$ on this panel (panel 5) was shown in Fig. 10. To obtain the curve in Fig. 13, the data were averaged over all α and N_{Re}. The data band is indicated by brackets. The values of $(h/h_0)_{max}$ increase with increasing δ and approximately double for each 10-deg increase in δ. These Mach 10 data are within 33% of the Mach 6 data up to $\delta = 15$ deg, but the Mach 6 data are much higher at $\delta = 20$ deg (compare Figs. 13 and 9, but note the scale difference). It is not evident from the heating contours why the Mach 6 data increased much more

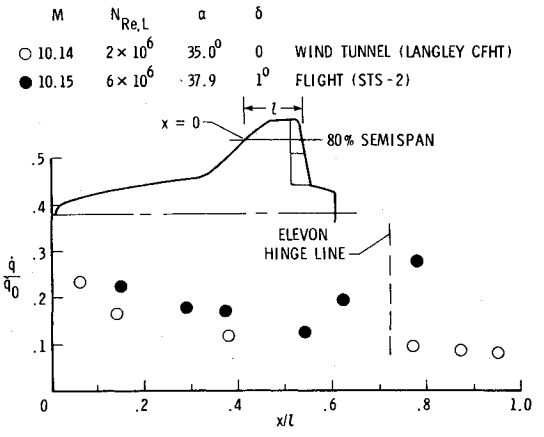

Fig. 14 Comparison of flight (STS-2) and wind tunnel (Langley CFHT) heat-transfer data.

than the Mach 10 data at large deflection angles. Flow visualization studies could possibly help explain this disparity.

Comparison to Flight

The nondimensionalized heating rate along a chord at approximately 80% semispan is shown in Fig. 14 for the undeflected-elevon wind tunnel model and the STS-2 (flight) Orbiter. The flight heating rate was obtained from Orbiter thermocouple data and use of the computational procedure outlined in Refs. 11-13. The flight reference-heating rate to the stagnation point of a full-scale 0.305-m (1-ft) radius sphere was obtained from the computational procedure of Ref. 14 which considers the equilibrium chemistry that is important in flight. The flight and wind tunnel conditions are shown on the figure where M, α, and δ are very nearly the same, but the flight $N_{Re,L}$ is about three times the wind tunnel value. Values of wind tunnel $\dot{q}$ would be on the order of 35% greater at the higher (flight) $N_{Re,L}$ based on the $\alpha = 35$ deg data of Fig. 10. This Reynolds number correction provides almost perfect agreement between flight and wind tunnel data over the first 55% of the chord. In flight, transition to turbulent flow apparently occurs at about 55% chord so that the heating rate increases over the remainder of the chord, whereas the wind tunnel values continue to decrease over that same length. Obviously, application of any wind tunnel data to a flight situation requires careful consideration of the relative flow environments.

Concluding Remarks

The phase-change paint technique was used to make heat-transfer measurements on five Space Shuttle Orbiter models with differentially deflected elevons. The outboard elevons were deflected windward through an angle δ when the inboard elevons were deflected through an angle -2δ, where $\delta = 0$, 5, 10, 15, and 20 deg. The models were tested in air at Mach 6 and 10 with two different flow conditions at each Mach number. Each test was run at three angles of attack: 20, 28, and 35 deg. This study was restricted to the windward side of the wing/elevon area. Based on these tests, and restricted to this range of study, the following conclusions are made.

The highest heating always occurs on the wing leading edge and at the inboard edge of the outboard, windward deflected elevon. Geometric patterns of heating on the wing and windward deflected elevons are often complex, particularly at 20 and 28 deg angles of attack. Multiple chordwise streaks of higher heating often occur across the wing and sometimes extend to spots of highly localized heating on the windward deflected elevon. In general, deflection of the elevons do not strongly alter these heating patterns on the wing. High heating near the leading edge of the wing is extended farther aft on the wing by the "streak" phenomena. In most, but not all,

cases, deflection of the elevons does not change the maximum heat-transfer coefficient anywhere on the wing by more than 40% of the values obtained where the elevons are undeflected at the same test condition and angle of attack. However, the maximum heat-transfer coefficient on the windward deflected elevon is a strong function of the deflection angle. For example, when data obtained in these tests were averaged over both test conditions and all angles of attack at each Mach number, the maximum heat-transfer coefficient on the 15 deg deflected elevon was approximately three times the value obtained on the undeflected elevon. Furthermore, multiplying factors for the coefficient between the undeflected and 20 deg deflected elevon were 4 at Mach 10 and 22 at Mach 6.

Acknowledgments

Thanks to H.H. Hamilton II for predicted data, D.A. Throckmorton for STS-2 flight heating-rate data, and H.R. Compton for STS-2 flight environment data.

References

[1]Findlay, J.T. and Compton, H.R., "On the Flight Derived/Aerodynamic Data Base Performance Comparisons for the NASA Space Shuttle Entries During the Hypersonic Regime," AIAA Paper 83-0115, 1983.

[2]Miller, C.G. III and Gnoffo, P.A., "Pressure Distributions and Shock Shapes for 12.84°/7° On-Axis and Bent-Nose Biconics in Air at Mach 6," NASA TM 83222, 1981.

[3]Goldberg, T.J. and Hefner, J.N. (Appendix by J.C. Emery), "Starting Phenomena for Hypersonic Inlets With Thick Turbulent Boundary Layers at Mach 6," NASA TN D-6280, 1971.

[4]Keyes, J.W., "Force Testing Manual for the Langley 20-Inch Mach 6 Tunnel," NASA TM-74026, 1977.

[5]Shaefer, W.T. Jr., "Characteristics of Major Active Wind Tunnels at the Langley Research Center," NASA TM X-1130, 1965.

[6]Jones, R.A. and Hunt, J.L., "Use of Fusible Temperature Indicators for Obtaining Quantitative Aerodynamic Heat-Transfer Data," NASA TR R-230, 1966.

[7]Creel, T.R. Jr., "A Device for Rapid Determination of Thermophysical Properties of Phase-Change Wind-Tunnel Models," NASA TM X-3421, 1976.

[8]Fay, J.A. and Riddell, F.R., "Theory of Stagnation Point Heat Transfer in Dissociated Air," *Journal of Aeronautical Sciences*, Vol. 25, Feb. 1958, pp. 73-85, 121.

[9]Hamilton, H.H., "Approximate Method of Predicting Heating on the Windward Side of Space Shuttle Orbiter and Comparisons with Flight Data," AIAA Paper 82-0823, June 1982.

[10]Herrera, B.J., "Results From a Convective Heat Transfer Rate Distribution Test on a 0.0175 Scale Model (22-0) of the Rockwell International Vehicle 4 Space Shuttle Configuration in the AEDC-VKF Tunnel B (OH49B)," Vol. 1 of 2, NASA CR-147, 626, 1976.

[11]Pittman, C.M. and Brinkley, K.L., "One-Dimensional Numerical Analysis of the Transient Thermal Response of Multilayer Insulative Systems," NASA TM X-3370, 1976.

[12]Bradley, P.F. and Throckmorton, D.A., "Space Shuttle Orbiter Flight Heating Rate Measurement Sensitivity to Thermal Protection System Uncertainties," NASA TM 83138, 1981.

[13]Wells, W.L. and Hudgins, J., "Experimental Assessment of a Computer Program Used in Space Shuttle Orbiter Entry Heating Analyses," NASA TM 84572, 1983.

[14]Hamilton, H. II, "Approximate Method of Calculating Heating Rates at General Three-Dimensional Stagnation Points During Atmospheric Entry," NASA TM 84580, 1982.